



Perfect Metamaterial Absorber

N. I. Landy,¹ S. Sajuyigbe,² J. J. Mock,² D. R. Smith,² and W. J. Padilla¹

¹*Department of Physics, Boston College, 140 Commonwealth Avenue, Chestnut Hill, Massachusetts 02467, USA*

²*Department of Electrical and Computer Engineering, Duke University, Durham, North Carolina 27708, USA*

(Received 6 November 2007; revised manuscript received 10 March 2008; published 21 May 2008)

We present the design for an absorbing metamaterial (MM) with near unity absorbance $A(\omega)$. Our structure consists of two MM resonators that couple separately to electric and magnetic fields so as to absorb all incident radiation within a single unit cell layer. We fabricate, characterize, and analyze a MM absorber with a slightly lower predicted $A(\omega)$ of 96%. Unlike conventional absorbers, our MM consists solely of metallic elements. The substrate can therefore be optimized for other parameters of interest. We experimentally demonstrate a peak $A(\omega)$ greater than 88% at 11.5 GHz.

DOI: 10.1103/PhysRevLett.100.207402

PACS numbers: 78.68.+m, 41.20.-q, 78.20.Ci

The nascent field of electromagnetic metamaterials (MMs) has produced exotic effects such as negative index of refraction [1,2], and devices such as an electromagnetic cloak [3]. The realization of such properties lies in the ability of metamaterials to create independent tailored electric [4] and magnetic [5] responses to incident radiation. Electromagnetic MMs are also geometrically scalable which translates into operability over a significant portion of the electromagnetic spectrum. To date, MMs have been demonstrated in every technologically relevant spectral range, from radio [6], microwave [7], mm-Wave [8], THz [9], MIR [10], NIR [11], to the near optical [12]. These designer materials are ideal for the investigation of novel emergent physical phenomena while also holding great promise for future applications.

As an effective medium [13], MMs can be characterized by a complex electric permittivity $\tilde{\epsilon}(\omega) = \epsilon_1 + i\epsilon_2$ and magnetic permeability $\tilde{\mu}(\omega) = \mu_1 + i\mu_2$. Much of the work in MMs has been focussed on the real part of ϵ and μ to enable the creation of a negative refractive material. However, the oft-overlooked loss components of the optical constants (ϵ_2 and μ_2) have much potential for the creation of exotic and useful materials as well. For example, they can be manipulated to create a high absorber. By manipulating resonances in ϵ and μ independently, it is possible to absorb both the incident electric and magnetic field. Additionally, by matching ϵ and μ , a MM can be impedance-matched to free space, minimizing reflectivity. In this Letter, we show that MMs can be fashioned to create narrow-band perfect absorbers (PAs), with the potential to be used in devices such as in bolometers.

A single unit cell of the absorber consisted of two distinct metallic elements as shown in Figs. 1(a) and 1(b). Electric coupling was supplied by the electric ring resonator (ERR) [14], shown in Fig. 1(a). This element consisted of two standard split ring resonators connected by the inductive ring parallel to the split-wire. We used this design instead of a conventional split-wire design because of the limitations of straight wire media [15]; i.e., a split-wire design has limited tunability beyond the addition of more wires per unit cell to increase inductance [16]. The

magnetic coupling required a more complicated arrangement, and thus in order to couple to the incident \mathbf{H} -field, we needed flux created by circulating charges perpendicular to the propagation vector. We created this response by combining the center wire of the ERR with a cut wire [Fig. 1(b)] in a parallel plane separated by a substrate [Fig. 1(c)]. This design is similar to the so-called “fishnet” and paired nanorod structures [11,12], in that they derive a magnetic response from driving two antiparallel currents in conducting segments. We were then able to tune the magnetic response by changing the geometry of the cut wire and the separation between the cut wire and electric resonator. By manipulating the magnetic coupling without changing the ERR, we were able to decouple ϵ and μ and individually tune each resonance.

We performed computer simulations of an ideal— but realizable—MM absorber using the commercial finite-difference time domain (FDTD) solver Microwave Studio by CST [17]. The program simulated a single unit cell as shown in Fig. 1(c) with appropriate boundary conditions, i.e., perfect electric ($\hat{y}\hat{z}$ -plane) and perfect magnetic ($\hat{x}\hat{z}$ -plane). Waveguide ports on the other boundaries simulated a TEM plane wave propagating through the medium. Simulation produced the complex frequency dependent S parameters, \tilde{S}_{11} and \tilde{S}_{21} , where $T(\omega) = |\tilde{S}_{21}|^2$ and $R(\omega) = |\tilde{S}_{11}|^2$ are the transmission and reflectance,

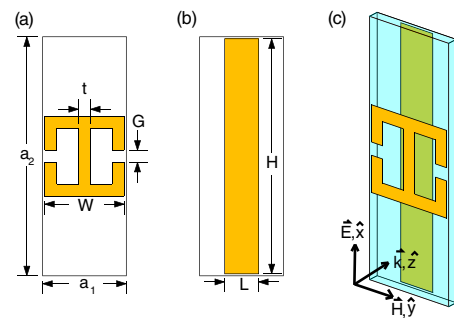


FIG. 1 (color online). Electric resonator (a) and cut wire (b). Dimension notations are listed in (a) and (b). The unit cell is shown in (c) with axes indicating the propagation direction.

respectively. From the S parameter data, we inverted the Fresnel equations to extract the complex optical constants [18]. We then examined the behavior of the surface current density, magnetic and electric fields at ω_0 to verify that we were coupling to the correct resonant mode of each MM element. By tuning ω_0 of the ϵ and μ resonances (not shown), due to the two MM elements, we achieved $\epsilon = \mu$ and thus an impedance near the free space value. While 100% absorbance is theoretically possible, it can only occur when the MM layer is impedance-matched to free space such that $R(\omega)$ is zero [19]. One may then minimize $T(\omega)$ such that the addition of multiple layers ensures $T(\omega) \rightarrow 0$. The simulated MM had the dimensions, in millimeters, of: $a_1 = 4.2$, $a_2 = 12$, $W = 3.9$, $G = 0.606$, $t = 0.6$, $L = 1.7$, $H = 11.8$, and the MM elements were separated by 0.65 in the \hat{z} direction. In Fig. 2, we show the simulation results for the MM PA. $R(\omega)$ and absorbance $[A(\omega)]$ are plotted from zero to 100% (left axis), and $T(\omega)$ is plotted on the right axis from zero to 5%. $R(\omega)$ is large $\sim 97\%$ near the bounds of the plot, 9 GHz and 14 GHz, but there is a minimum of 0.01% at $\omega_0 \equiv 11.65$ GHz. Simulated $T(\omega)$ also undergoes a minimum near ω_0 and yields a value of $\sim 0.9\%$. Thus, we achieve a best simulated $A(\omega) = 1 - T(\omega) - R(\omega)$ slightly less than unity $A(\omega) = 99\%$ with a FWHM of 4% compared to ω_0 .

While our simulated absorber achieves narrow-band high $A(\omega)$, we were restricted by the minimum line widths available to us (250 μm) and other various fabrication tolerances. These limitations were incorporated into the design process, and we fabricated a MM which deviated slightly from the ideal absorber and had the dimensions, in millimeters, of: $a_1 = 4.2$, $a_2 = 12$, $W = 4$, $G = 0.6$, $t = 0.6$, $L = 1.7$, $H = 11.8$. Each metallization was fabricated on a FR4 substrate with a thickness of 0.2 mm. MMs were fabricated using standard optical lithography. The substrate consisted of a photosensitized FR-4 board with a 17 μm copper thickness. A mask was designed and printed in high resolution on a transparency, and each MM component was fabricated by standard optical lithography processes. These boards were then sandwiched (using an adhesive with 0.06 mm thickness) about another 0.2 mm thick FR4 blank substrate to obtain the correct spacing. The end results was that the MM elements were separated by 0.72 mm in the \hat{z}

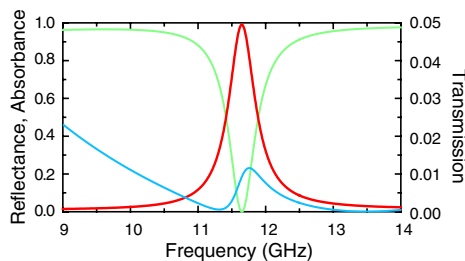


FIG. 2 (color online). Simulated MM PA. $R(\omega)$ (light gray line, green online) and $A(\omega)$ (black line, red online) are plotted from zero to 100% (left axis). $T(\omega)$ is plotted on the right axis as the gray line (blue online) on a scale from zero to 5%.

direction. This allowed us to couple to both magnetic and electric resonances without out-of-plane elements typical with “wine-crate” designs [2].

We experimentally verified the behavior of the absorber by measuring the complex S parameters of a large planar array of pixels (outer dimensions of 15×15 cm). We used a vector network analyzer that produced microwaves in the range of 8–12 GHz. One microwave horn focused the GHz beam on the sample, and another horn served as a detector. Both horns coupled to linearly polarized light and had parallel polarization directions. To measure $T(\omega)$, we set the horns in a normal incidence confocal configuration. We performed $R(\omega)$ measurements at normal incidence. However, in order to eliminate large voltage standing wave ratios (VSWR) which would overwhelm the data, we used a beam splitter configuration, shown as the inset to Fig. 3(a). Radiation first traveled from the transmitting horn through the beam splitter, reflected from the sample and returned to the beam splitter where it was reflected at 45% to the receiving horn. We set the normalization and phase in $T(\omega)$ configuration by simply removing the sample. For reflection, we replaced the sample with a perfect reflector for normalized measurements. Transmission techniques have been described elsewhere [20].

Simulations were performed for this MM structure and are presented for comparison to experimental data. $R(\omega)$ is shown as the black (red online) line in Fig. 3(a). At low frequencies, the reflectivity is high and yields values near 95%. A large feature occurs in $R(\omega)$ and has a minimum of $\sim 3\%$ near 11.5 GHz. Likewise, $T(\omega)$, shown as the black (red online) line in Fig. 3(b), has 4% $T(\omega)$ at low frequencies and then undergoes a minimum near 11.25 GHz. $A(\omega)$ of our MM unit cell thus has a maximum near where both $R(\omega)$ and $T(\omega)$ have their minima. We plot $A(\omega)$ as the

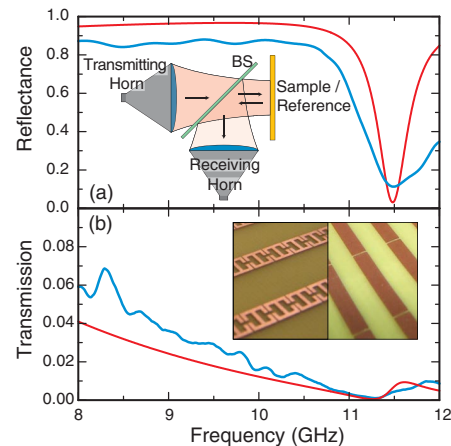


FIG. 3 (color online). Simulated (black lines, red online) and measured (gray lines, blue online) $T(\omega)$ and $R(\omega)$ for the microwave absorber. (a) Displays $R(\omega)$ from zero to 100%. A schematic of the reflection experiment is shown as the inset to (a) where BS is the beam splitter. $T(\omega)$, shown in (b), are displayed from zero to 10%. Inset to (b) shows photographs of the both sides of the MM absorber.

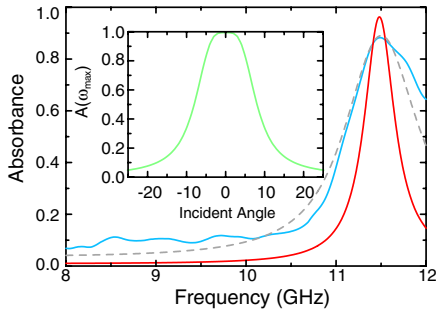


FIG. 4 (color online). Main panel shows the simulated (black line, red online) and measured (gray line, blue online) $A(\omega)$ lines. The dashed gray $A(\omega)$ line is a Gaussian weighted average which approximates assembly error. Inset shows the simulated angular dependence of the $A(\omega)$ at ω_{\max} .

black (red online) line in Fig. 4 from 8 to 12 GHz. Simulated $A(\omega)$ peaks at 96% at $\omega_0 = 11.48$ GHz and has a FWHM of 4% with respect to ω_0 .

By performing S parameter simulations, we are able to account for the form of the experimental data. The measured $R(\omega)$ and $T(\omega)$ are plotted as the gray (blue online) lines in Figs. 3(a) and 3(b), respectively. We find excellent agreement between simulated and measured $T(\omega)$ over all frequencies characterized. The measured $R(\omega)$ is consistently 8% lower than the simulated $R(\omega)$ at low frequencies. Both the simulated and experimental $R(\omega)$ reach a minimum at approximately 11.5 GHz, but experimentally, the minimum is 11%, as opposed to the simulated value of 3%. There is also significant broadening in the experimental $R(\omega)$ line with respect to simulation. This is most likely due to tolerances in the fabrication and assembly.

The experimental absorptivity $A(\omega)$ calculated from $T(\omega)$ and $R(\omega)$ is shown as the gray (blue online) line in Fig. 4. The simulated and experimental lines have maximum $A(\omega)$ at the same frequency, $\omega_{\max} = 11.5$ GHz. However, the simulated line reaches a maximum of 96%, and the experimental line only reaches 88%, the difference being primarily due to deviations in $R(\omega)$. Better fabrication and assembly tolerances will permit absorbances and bandwidths similar to that shown as the black (red online) line in Fig. 4. We performed simulations to verify the origin of the broadening of $A(\omega)$. From a theoretical viewpoint, it is expected that the frequency location of the $A(\omega)$ peak depends significantly upon the separation between the electric ring resonator and the cut wire, since this distance determines the frequency location of the magnetic resonance. Simulations verified this conjecture. We simulated various spacings centered about the designed value of 0.72 mm, and computed a Gaussian weighted average $A(\omega)$ with a standard deviation of $\sigma = 20 \mu\text{m}$. The $A(\omega)$ calculated in this manner agrees very well with the experimental line and is plotted as the gray dashed line in the main panel of Fig. 4. Thus, assembly errors in the MM spacing of only 5% can easily account for the disagreement

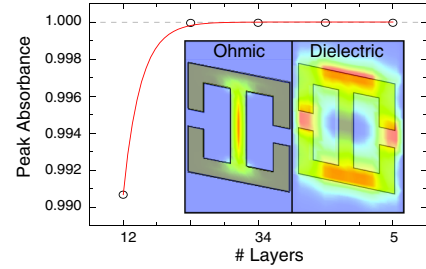


FIG. 5 (color online). Simulated $A(\omega)$ with increasing MM layers; line is a guide to the eye. Insets show the simulated losses at resonance. The Ohmic loss (surface) is shown in the left inset panel, and the dielectric (volume) loss is on the right.

between the simulation and experiment shown in Fig. 4 as the black and gray (red and blue online) lines, respectively.

An investigation into the effect of adding multiple MM absorbing layers is shown in the main panel of Fig. 5. As can be observed, $A(\omega)$ rises sharply with additional layers and is asymptotic to unity, within computational noise. Two layers of the MM absorber achieve a value of $\sim 99.9972\%$. At this thickness, the entire MM is only $\sim \lambda_0/2$ at resonance. For the structure shown in Fig. 1, $A(\omega_0)$ can never reach unity since the MM is not perfectly matched to free space. However, it is important to note that although an impedance-matched structure may yield zero $R(\omega_0)$, this does not imply $T(\omega_0) = 0$. In this study, we are interested in achieving $R(\omega_0) = T(\omega_0) = 0$ in a single unit cell in the propagation direction. Thus, our MM structure was optimized to maximize the $A(\omega)$ with the restriction of minimizing the thickness. If this constraint is relaxed, impedance matching is possible, and with multiple layers, a perfect $A(\omega)$ can be achieved.

We further investigated the origin of the loss in our MM, as indicated in the inset to Fig. 5. The Ohmic “surface” loss is mainly from the center conducting region of the ERR, and dielectric losses occur in between the two MM elements where the electric field is large. The major component responsible for $A(\omega)$ in our MM structure is the dielectric loss, and simulation indicates this is an order of magnitude greater than Ohmic losses. This is consistent with studies of frequency selective surfaces (FSSs) where it was found that metallic absorption was relatively insignificant in comparison to dielectric losses [21].

We now discuss the potential application of a perfect MM absorber as a bolometer. An ideal bolometric detector is one in which all photons that fall upon its surface are absorbed, converted to heat, and thus sensed [22]. A prominent feature of commercially available bolometers is their extreme bandwidth making them ideal candidates as detectors, especially in the far infrared frequency regime where other efficient detection methods are largely unavailable. However, bolometers which achieve a narrow band response also have significant application as focal plane array (FPA) detectors for imaging. The MM design presented here achieves simulated absorptivities near unity

making them ideal candidates for bolometric pixel elements. The natural narrow band MM resonance is a salient feature for FPA detectors as it is naturally apodizing and operates at room temperature. Since the elements which constitute our bolometer are subwavelength, MMs can inherently image at the diffraction limit. Further, here we have used only a *single unit cell* in the propagation direction, (with a thickness significantly smaller than the wavelength $\lambda_0/35$), yet achieved an experimental $A(\omega) = 88\%$. By adding multiple layers, one can achieve narrow band absorbance of unity. Although the design is planar and $A(\omega)$ should fall off relatively rapidly, we investigated the angular dependence (inset to Fig. 4) and found the MM still achieved $A \approx .5$ at an incident full-angle of 16° . Finally, MM scalability permits the usage of these PAs at other wavelengths of interest, allowing for the possibility of room temperature high resolution imaging at mm-Wave and THz frequencies. We have designed similar MMs (not shown) that achieved $A \approx 1$ operating at 94 GHz and 1 THz.

While the creation of a MM absorber is novel, the technology to create absorptive materials in the microwave frequency range is well established. A high-impedance ground plane yields comparable absorbance, but requires metalization in the propagation direction [23]. The material “chiroshield” is capable of very high absorption, and reduces backscatter by 15 to 25 dB [24], but has sizes on the order of λ , which is 35 times larger than our design at a given center frequency. Some ferrites show reflection loss of -30 dB [25]; however, they lack the inherent and precise tunability of MMs. Other work on bolometric frequency-selective materials require cryogenic temperatures to operate and only achieve $A(\omega) = 50\%$ [26]. At optical, metal colloides are known to have large absorptive properties [27] due to the geometric specific surface modes [28]. This suggests an interesting possible application of artificial plasmonic wire media [4] to function as PAs [16] operating at microwave frequencies.

In conclusion, we have demonstrated that MMs can be highly absorptive over a narrow frequency range. This stems from the ability to design MM elements which can individually absorb the electric and magnetic components of an incident electromagnetic wave. In contrast, previous experimental results at THz frequencies using a single type of MM element (electric) yielded values of only $A(\omega) \approx 20\%$ [29]. The resonant frequency of the MMs may be tuned throughout some range of frequencies [30,31] thus enabling hyperspectral imaging. A further benefit afforded by MMs is the ability to construct a single unit cell with $\mu(\omega) = \epsilon(\omega)$ over an extended frequency range. Thus, this unit cell can achieve zero $R(\omega)$ since it can have an impedance equal to the free space value $Z = \sqrt{\mu/\epsilon} = 1$. This is similar to the well-known theoretical construct, the Perfectly Matched Layer (PML) Absorbing Boundary Condition (ABC) [32], which splits waves incident upon a boundary into electric and magnetic components to ob-

tain near perfect absorption. The PML, however, requires gain and additionally is on the order of $\lambda_0/2$ in thickness [33].

The design presented here can still be improved. The current design is polarization sensitive, which is not ideal for some applications. By incorporating a substrate with a highly consistent dielectric constant, we will be able to optimize the design at the correct resonant frequency. Similarly, tighter fabrication tolerances would allow us to bring the impedance closer to unity and therefore closer to $A(\omega) = 1$. Additionally, the assembly is complicated due to the restrictions placed on the direction of the incident wave to couple to the magnetic resonator. This resulted in unit cell variation and a less distinct $A(\omega)$ peak.

N. I. L. and W. J. P. acknowledge support from the Los Alamos National Laboratory LDRD program, D. R. S. acknowledges support from MDA Contract No. W9113M-07-C-0078, and D. R. S., S. S., and J. J. M. acknowledge support from a MURI sponsored by the Air Force Office of Scientific Research Contract No. FA9550-06-1-0279.

-
- [1] V. G. Vesalago, *Sov. Phys. Usp.* **10**, 509 (1968).
 - [2] R. A. Shelby *et al.*, *Science* **292**, 77 (2001).
 - [3] D. Schurig *et al.*, *Science* **314**, 977 (2006).
 - [4] J. B. Pendry *et al.*, *Phys. Rev. Lett.* **76**, 4773 (1996).
 - [5] J. B. Pendry *et al.*, *IEEE Trans. Microwave Theory Tech.* **47**, 2075 (1999).
 - [6] M. C. K. Wiltshire *et al.*, *Science* **291**, 849 (2001).
 - [7] D. R. Smith *et al.*, *Phys. Rev. Lett.* **84**, 4184 (2000).
 - [8] M. Gokkavas *et al.*, *Phys. Rev. B* **73**, 193103 (2006).
 - [9] T. J. Yen *et al.*, *Science* **303**, 1494 (2004).
 - [10] S. Linden *et al.*, *Science* **306**, 1351 (2004).
 - [11] S. Zhang *et al.*, *Phys. Rev. Lett.* **95**, 137404 (2005).
 - [12] G. Dolling *et al.*, *Opt. Lett.* **32**, 53 (2007).
 - [13] D. R. Smith *et al.*, *J. Opt. Soc. Am. B* **23**, 391 (2006).
 - [14] W. J. Padilla *et al.*, *Phys. Rev. B* **75**, 041102(R) (2007).
 - [15] D. Schurig *et al.*, *Appl. Phys. Lett.* **88**, 041109 (2006).
 - [16] D. R. Smith *et al.*, *Appl. Phys. Lett.* **75**, 1425 (1999).
 - [17] CST Studio Suite 2008, CST of America. (2008).
 - [18] D. R. Smith *et al.*, *Phys. Rev. B* **65**, 195104 (2002).
 - [19] S. G. Johnson *et al.*, *Phys. Rev. E* **66**, 066608 (2002).
 - [20] A. F. Starr *et al.*, *Phys. Rev. B* **70**, 113102 (2004).
 - [21] J. E. Reynolds *et al.*, *J. Appl. Phys.* **93**, 5346 (2003).
 - [22] P. L. Richards, *J. Appl. Phys.* **76**, 1 (1994).
 - [23] Q. Gao *et al.*, *Electron. Lett.* **41**, 936 (2005).
 - [24] I. V. Lindell *et al.*, *Electromagnetic Waves in Chiral and Bi-Isotropic Media* (Artech House, Norwood, MA, 1994).
 - [25] P. Singh *et al.*, *Mater. Sci. Eng. B* **78**, 70 (2000).
 - [26] T. A. Perera *et al.*, *Appl. Opt.* **45**, 7643 (2006).
 - [27] W. Lamb *et al.*, *Phys. Rev. B* **21**, 2248 (1980).
 - [28] J. B. Pendry, *J. Mod. Opt.* **41**, 209 (1994).
 - [29] J. F. Ohara *et al.*, *J. Nanoelectron. Optoelectron.* **2**, 90 (2007).
 - [30] W. J. Padilla *et al.*, *J. Opt. Soc. Am. B* **23**, 404 (2006).
 - [31] H.-T. Chen *et al.*, *Nat. Photon.* (to be published).
 - [32] J. Berenger, *J. Comp. Physiol.* **114**, 185 (1994).
 - [33] A. Taflov *et al.*, *Computational Electrodynamics: The Finite-Difference Time-Domain Method* (Artech House, Norwood, MA, 2000), 3rd ed.